

Quantum gas-enabled direct mapping of active current density in percolating networks of nanowires

J. Fekete,^{*,†} T. M. James,[†] R. Shah,[†] A. Gadge,[†] S. Bhumbra,[†] F. Oručević,[†] and P. Krüger^{†,‡}

[†]*Department of Physics and Astronomy, School of Mathematical and Physical Sciences, University of Sussex, Brighton, BN1 9QH, United Kingdom*
[‡]*Physikalisch-Technische Bundesanstalt, 10587 Berlin, Germany*

E-mail: J.Fekete@sussex.ac.uk

Abstract

Electrically percolating networks made of nanowires are amongst the most promising candidates for next generation transparent electrodes. The inherent heterogeneity of the spatial distribution of current in these materials is at the centre of interest for development as it leads to phenomena like re-routing of the percolation pathways or localized self-heating, which may result in irreversible damage. In the absence of an experimental technique that can spatially resolve the current distribution and a nonlinear percolation model suitable to interpret it, one relies on empirical rules and safety factors to engineer these materials.

In this paper, we introduce a novel quantum sensing technology as a solution to the long standing problem of imaging active current flow in 2D electrically conductive materials. We report on Bose-Einstein condensate microscopy (BEC-M) achieving the performance and technology levels where investigating the dynamic re-distribution of current pathways in electrically percolating networks becomes feasible. Better measurement and understanding of the networks can have far reaching consequences. We show that the current density characterization, combined with existing thermal imaging methods, will for the first time

avoid intermediate assumptions on the link between thermal and conductive properties in these nonlinear networks. This will enable testing and modeling individual junction behaviour and hot spot formation over the network. Investigating reversible and irreversible mechanisms will aid the development of devices with better macroscopic performance and higher stability and reliability.

Keywords

Transparent conductive materials, silver nanowires, percolation networks, active current density imaging, quantum technology, ultrasensitive magnetometry

Introduction Over the last few decades electrical percolating networks have attracted much interest, especially since they have gained an increasingly important role in the development of transparent conductors,¹ flexible thin-film transistors² and chemical³ and nanobio⁴ sensors. Percolation theory takes a statistical approach to characterise the relationship between the microscopic structure and the macroscopic physical properties of these networks. This theory has successfully described counterintuitive responses and provided scaling laws for network properties such as electrical conductance and

maximum voltage drop.^{5–7} As some of the main parameters of the networks can be continuously tuned, they are ideal test beds for percolation models, which in turn help to optimise network performance in the applications.

In the study of electrical percolating networks, arguably the biggest remaining challenge originates in the absence of a non-invasive experimental technique that could directly reveal a spatially resolved current density pattern and its (often nonlinear) dynamic changes when a voltage is applied across the network. Such a tool, especially when used in combination with existing ones, would enable in-depth studies of the interplay between electrical, thermal and surface properties, bridging the gap between network-scale properties and microscopic observations.

The absence of a viable direct microscopic current density imaging technique has stimulated alternative, indirect measurements of the current flow. Scanning electron microscopes, atomic force microscopes (AFM) with conductive, Kelvin-probe or magnetic force modules provide detailed information on the topography, important surface properties and conductivity.⁸ Recently, thermal imaging has been shown to be an efficient tool to study percolating networks^{9–11} with thermal maps being recorded during active current flow in a network. This method revealed interesting mechanisms in hot spot formation and clustering. For the interpretation of the measurements the relationship between local current density and temperature relies on assumptions, which only hold in the low current density limit. The thermal changes in the network are only detectable, however, when current densities are high, because the sensitivity of existing methods is low. In this regime nonlinear thermo-electric interactions in the network are significant, which requires more complex models (see discussion later in this paper).

Here we introduce a solution to the long-standing problem of current density mapping of random two-dimensional (2D) networks. Our approach exploits the capability of quantum gases, such as Bose-Einstein condensates (BEC), to sense ultra-low magnetic

fields. BEC microscopy (BEC-M)^{12–14} offers a unique combination of microscopic resolution, sub-nanoampere sensitivity, and tunable dynamic range. In addition, it is possible to map active current distributions in a single imaging shot rather than having to rely on a time-consuming multi-step scan. These properties make this method an outstanding candidate to explore the nonlinear phenomena in electrical percolating networks.

In this Letter we demonstrate the feasibility and analyze the capability of the BEC-M technique in the study of electrical percolating networks in the key test case of silver nanowires. We report on benchmark experiments on a microfabricated planar reference structure demonstrating a substantial improvement over the state of the art. We illustrate that at this performance level the method is fully viable for current density mapping in percolating networks by simulating BEC-M data obtained from different density random nanowire networks. We discuss the key advantages of data acquired with this technique over the information obtained by the different modalities of the widely used AFMs. Furthermore, using a single junction model, we show how BEC-M has the potential to deepen our understanding of the thermo-electric interplay in these networks, which is responsible for important phenomena including self-heating and reconfiguration of current pathways. In the context of the challenge of investigating nonlinear percolating networks,^{7,10} we further outline how the technique can be used to study nonlinear phenomena and observe dynamics including reversible as well as irreversible mechanisms (see example shown in Figure 4a).^{11,15,16}

BEC microscopy Since their prediction¹⁷ (1924) and first experimental observations¹⁸ (1995), BECs have recently attracted much attention in quantum sensing applications, since they are outperforming their classical counterparts in various fields.^{12,19–21} BEC-M has been introduced^{12,22–25} as a technique to measure the local variation in the magnetic field. It has first been demonstrated with fields emanating from current-carrying microfabricated

structures. The method relies on atom chip technology²⁶ to precisely control and manipulate ultracold gases including BECs near surfaces. Small changes in the local magnetic field cause density variations of the atomic gas, which can be directly related to variations in the current flow direction. This effect has been measured in lithographically fabricated (evaporated)²⁵ and electroplated wires²⁷ as well as in microstructured patterns.¹³ It has also been used to observe the nematic transition in iron pnictide, a high-temperature superconductor.²⁸

Working principle Neutral atoms in an ultrahigh vacuum environment are initially laser cooled before being magnetically trapped and then further cooled by forced evaporation below the critical temperature for Bose Einstein condensation (typically hundreds of nanokelvins).¹⁸ The magnetic trapping relies on precisely controlled currents (in atom chips, printed circuit boards (PCB), mm-thick wires, coils) to produce the magnetic field of desired spatial distribution. As atoms are being trapped in the regions of the lowest magnetic potential (proportional to the field magnitude), this allows for flexible manipulation of the atomic probe to vary its shape and position in the three-dimensional space. An elongated cigar shaped (quasi one-dimensional, 1D) ultracold atomic cloud is prepared on an atom chip for microscopy measurements. Figure 1a depicts such a cloud above the trapping structure and typical field lines of the magnetic trap in the y - z plane, which serves for the tight radial confinement of the atoms.

A sample of interest is placed between the trapped atoms and the trapping structure. Minute magnetic fields emerging from the sample are sufficient to modify the magnetic potential and with it the confinement for the atoms. The atomic wavefunction (and therefore atomic density distribution) is distorted in response, and can be recorded with standard imaging methods on a camera. See Figure 1b for a schematic illustration of BEC-M operation.

The field distribution emanating from the sample can be reconstructed along the 1D probe (along x) from a single shot image taken in a

fraction of a millisecond. A 2D-field map can be created by raster scanning the probe position along the orthogonal direction y over the sample surface. Each field recording involves the re-creation of the atomic probe and its destructive imaging with a duty cycle on the order of seconds. The density variation of the cloud (even fragmentation) is a consequence of field variation primarily along x , the long axis of the cigar shape cloud. As the field decays with the distance from its source, closer to the surface this variation is stronger, i.e. the sensitivity to current improves.

Current density mapping We have recorded a set of atomic distributions as their position was scanned across the surface (over a range of $80\ \mu\text{m}$ in $4\ \mu\text{m}$ steps along y , just above a $200\ \mu\text{m}$ wide, $2\ \mu\text{m}$ thick gold track of the chip in Figure 1a), while keeping the trap shape (22 Hz longitudinal and $\gtrsim 1.4\ \text{kHz}$ radial frequencies of a harmonic trap), the field minimum ($130\ \mu\text{T}$) and distance to the surface ($1.4\ \mu\text{m}$) constant. The atoms were cooled well below the critical temperature for Bose Einstein condensation and their distribution was subsequently imaged. For simplified quantitative analysis, the trapping potentials are switched off 1 ms before the images are taken without any fields present. Such short free evolution does not affect the relevant atomic distribution profile.

The measured atomic distributions were converted into atomic line densities $n_{1\text{D}}(x)$, as shown in Figure 1c as a function of the y position. From the line densities, the change in magnetic field component B_x , can be approximated by $2h\nu_\perp a_{sc}/\mu_B \cdot \delta n_{1\text{D}}(x)$ in the low density limit ($n_{1\text{D}} < 100\ \text{atoms}/\mu\text{m}$), as shown in Figure 1d.²⁹ Here h is Planck's constant, ν_\perp is the radial trapping frequency, a_{sc} is the s-wave scattering length, μ_B is the Bohr magneton.

The current density J_y (leading to the field variation in the orthogonal direction) is then calculated from the measured magnetic field distribution using an inverse method, see Figure 1e. The lines with arrows represent 'current flow', the density of lines is proportional to the change in current density.

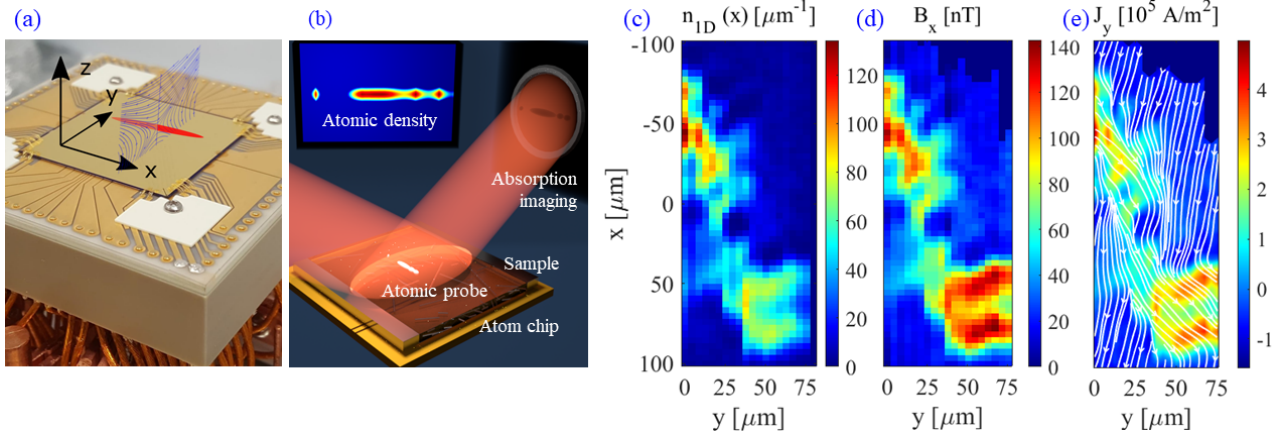


Figure 1: (a) Trapping structure (PCB and atom chip) and illustration of magnetic field lines in the y - z plane of a magnetic quadrupole forming a trap used for the radial confinement of the atomic probe. (b) BEC-M operation scheme. (c) A raster scan of atomic line densities $n_{1D}(x)$ measured over a planar micro-fabricated conductor. (d) Magnetic field distribution and (e) current density calculated from (d). The lines with arrows represent current flow, the density of lines is proportional to the current density J_x with a factor 1000 enhancement with respect to J_y for visibility.

The single shot noise floor for these measurements was 0.177 atoms/ μm , which converts to a minimum detectable field of $\delta B_x = 178 \text{ pT}$. The maximum field value of 137 nT indicates a dynamic range of 770. The sensitivity to current is 1.25 nA assuming an infinitely thin wire as the source of the field. As the source dimensions increase, the minimum detectable current increases. On the other hand, if the thickness of the current carrying structure is negligible compared to its distance to the atoms, but the width is significant, then the minimum detectable current density is a more appropriate performance measure, and improves for wider structures. In the case of a random nanowire network, the wires can be well approximated by infinitely thin wires for estimating the sensitivity of BEC-M.

It is interesting to note that we have observed field variations as large as 8 nT/ μm (when averaged over 3 repeats). In principle, this allows as low as 22 nm probing step size while detecting finite changes in the magnetic field (considering only the field detection limit). At the noise level of existing power supplies used for trapping (limited by current technology), this is not possible, though.

More importantly, the cloud size (radii of 290 nm radially and 34 μm longitudinally) de-

termines the ultimate spatial resolution and the ‘field of view’. The resolution of the BEC-M is limited by two parameters. Along the linescan, x , the resolution is limited by optical diffraction to typically a few micrometres due to long working distances. In the y direction, the precise control of the position and the tight radial confinement of the atoms set the effective resolution as the radial size of the cloud, which is proportional to $1/\sqrt{\nu_{\perp}}$. The orientation of the atomic probe and the scanning direction can be changed by 90° if high resolution is required in both directions. By tightening the radial confinement, one can further improve the resolution, however, at the cost of reduced field sensitivity ($\propto \nu_{\perp}$), e.g. a 100 nm resolution would correspond to a field sensitivity of 1.5 nT.

To put these performance values into context, it is worth to compare field sensitivities of all existing magnetometers. State of the art magnetic field sensors are dominated already by quantum sensors, but there is a trade-off between sensitivity and spatial resolution.^{13,30} The sensors with the highest sensitivity operate in the millimetre to centimetre range, and sensors that can resolve magnetic field variation at nanoscale have orders of magnitude lower sensitivity. For measuring DC magnetic fields emanating from direct current sources, the BEC-M

offers the best performance in terms of sensitivity in the microscopic range among all existing technologies.

Percolating networks We demonstrate the feasibility of the BEC-M on nanowire networks of different densities, at operating conditions similar to the measurements described above (see Figure 2). Randomly generated networks of silver nanowires with 120 nm diameter are subject to $1 \mu\text{A}$ input current, and the current density is reconstructed for a radial trapping frequency of $\nu_{\perp} = 1 \text{ kHz}$ at an atom-surface distance of $1 \mu\text{m}$. Figure 2 shows the randomly generated and the reconstructed current density distribution, for a network close to the percolation threshold as well as for a high density network. The network density is related to the transparency of the sample,³¹ the transmittance of the two cases are 90% and 80%, respectively.

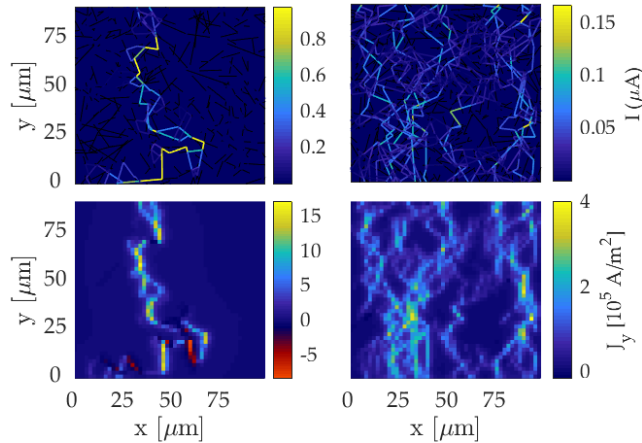


Figure 2: Randomly generated nanowire network models with transmittances of 90% (left) and 80% (right subfigure). Colours show the current in each wire (no current in the black wires). Figures in the lower panel show the reconstructed current density distributions from their respective networks. The input current to the networks was $1 \mu\text{A}$, and the upper and lower edges of the $100 \mu\text{m} \times 100 \mu\text{m}$ area represent the two electrodes.

These examples show that it is possible to distinguish individual current paths and junctions even well above the percolation threshold

for standard operating conditions of the BEC-M. One can also observe sections with reverse direction of the current flow, information that other methods are not able to reveal. In the 80% transmittance case hot spots are visible and the current paths can still be resolved.

Method comparison To demonstrate the advantages of BEC microscopy –measuring active current flow as opposed to conductivity–, we compare the simulated BEC-M current density map to experimental data measured on a small section of a nanowire network by atomic force microscope. The topography scan (Figure 3a) reveals that these nanowires have approximately 30 nm diameter and typically $> 10 \mu\text{m}$ length. Figure 3b is the corresponding measurement in conductive AFM (C-AFM) mode. From the two figures one can identify dead-ends which do not carry any current in a live network (the network formed when electrodes on the opposite sides of the sample are connected), but show up in the C-AFM due to the path from the bias electrode (towards the bottom of the figure) to the AFM tip closing the circuit. One can also notice that the measured current value is very sensitive to the tip position relative to the nanowire axis, resulting in a discontinuous map. Therefore, the measured current cannot be expected to be proportional to the current in a live network. Besides this issue, the sensitivity and dynamic range are not appropriate to inform us of the presence of hot spots in a network, especially of those forming at low bias voltages.

In contrast to the C-AFM measurement, the current density image provided by the BEC-M reveals the active current paths only and shows no false connection at dead-ends. Absolute measures of the current density can be evaluated if the topography is known, and has a dynamic range at least two orders of magnitude above the minimum detection limit. Figure 3c was simulated by using the network topography in Figure 3a with known nanowire resistivity, assuming a typical junction resistance value of 100Ω and 100 nA input current applied to the network section (via two electrodes at the top and bottom edges). This represents a realistic

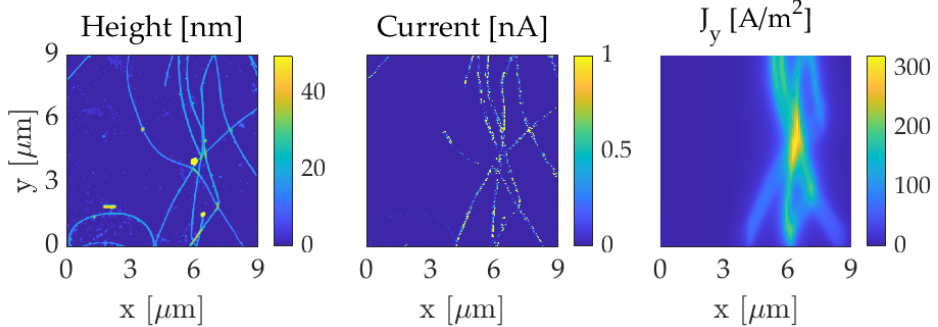


Figure 3: (a) Height map of a silver nanowire network section measured by AFM and (b) current map recorded by C-AFM. (c) Reconstructed active current density map from the simulation of BECs 100 nm above the network for the same topography for 100 nA input current.

example of a section where a hot spot can form within a larger network. The presence of multiple junctions with higher resistance than that of a nanowire segment of equivalent area gives rise to hot spot formation, which is the case for the simulated current map (Figure 3c).

For the simulation displayed in Figure 3c the topography was converted manually into segments of straight nanowires while for Figure 2 they were randomly generated. The current was attributed to the networks following Kirchoff's law with bulk silver resistivity and assuming 100Ω junction resistance. The current distribution produces a magnetic field distribution at a specified distance given by the Biot-Savart law. This magnetic field modifies the trapping potential for the atoms and leads to an atomic density variation within the 1D probe. The sensitivity to the magnetic field and spatial resolution can be determined from the trapping configuration and current values. With these parameters, the magnetic field affecting the atoms is used to calculate the current distribution in the sample by an inverse method based on the Green function. The method gives a unique solution with the assumption that the source is restricted to 2D, which is the case for nanowire networks where the atoms-sample distance is much greater than the sample thickness.

An additional unique feature of the BEC-M method is its ability to detect fast dynamical changes in current density distributions. The typical measurement cycle consists of (1) a few

seconds of preparation of the ultracold gas, (2) millisecond scale quantum dynamics following the atoms' response to any changes (e.g. voltage applied across the sample electrodes) and (3) tens of microseconds of imaging. During the preparation stage there is no need for current flow through the sample. The precise timing of the second and third stages in the experimental sequence together with controlled sample current, enables the observation of changes in current density patterns and transient effects on millisecond timescales in the sample through stroboscopic imaging of the atoms. When aiming to observe irreversible changes in the sample, imaging techniques that preserve the atomic probe during the sequence ('non-destructive imaging') can be employed to record the transient effect with higher repetition rate.

Nonlinearity in percolating networks It is interesting to look at percolating networks in terms of the thermo-electric interplay within and between its components. The microscopic observations of single nanowire and single junction resistances³² as well as those obtained by thermal imaging¹⁰ still fail to explain the non-Ohmic – also termed as super-Joule – behaviour of junctions, which forms the basis for models aiming to reproduce the dynamical current path redistribution over the network.¹⁰ Furthermore, the rich dynamics at microscopic scales are not necessarily reflected in macroscopic observations, as in the example where substantial reconfiguration of currents does not lead to ap-

preciable change in the total resistance of the network.

In this section we show how such reconfiguration of the networks can be understood via Joule heating of the wires and non-linear junction response to the temperature. We assume temperature-dependent bulk resistance of wires w_i [$R_{w_i}(T)$] and introduce an abrupt drop in junction resistance [$R_{J_j}(T)$] at a certain temperature. $R_{J_j}(T)$ has not been characterised extensively, but this model is consistent with the measurements of Bellew et al.³² For a given topology, a model describing $R_{J_j}(T)$ correctly should be able to predict the behaviour of the whole network. From the BEC-M data recorded in conjunction with thermal images at various current levels, one can determine $R_{J_j}(T)$ and gain insight into the percolating network behaviour.

We demonstrate a case of thermo-electrically induced current path reconfiguration using a simple model of two wires in contact at junction J (Figure 4b-c). The contact resistance of the junction is set to change abruptly from 600Ω to 10Ω as the temperature rises from 40°C to 44°C (blue solid line in Figure 4c). For a fixed current I_0 between the electrodes E1 and E2, we calculate the temperature and resistance along the segments of the two wires taking into account Joule heating, the heat diffusion and the temperature dependence of resistivity. The junction takes up the temperature of the local wire segment, while the electrodes E1 and E2, acting as thermal bath, maintain the temperature of wire ends at T_0 . For these calculations the silver wires are 60 nm in diameter and the wire sections corresponding to resistances R_0 , R_1 and R_2 are, respectively, $200 \mu\text{m}$, $100 \mu\text{m}$ and $80 \mu\text{m}$ long.

The ratio of currents in the two wire sections between E2 and J depends on the input current I_0 . For low I_0 , wire B carries less current ($I_2 < I_1$) due to the large junction resistance. For larger currents ($I_0 > 20 \mu\text{A}$) the situation is reversed and $I_2 > I_1$ as shown in the upper panel of Figure 4d.

This current path reconfiguration, due to the nonlinear junction response $R_{J_j}(T_j)$, brings the system into the regime of super-Joule heating.

Indeed, unlike the Joule heating power $P_1 = R_1 I_1^2$ which approximately scales with I_1^2 , $P_2 = (R_2 + R_j) I_2^2$ is qualitatively different from I_2^2 (see lower panel of Figure 4d).

Thermal imaging provides maps of the Joule heating power, but it does not give access to resistance or current information in the network independently. By obtaining the active current maps by BEC-M, the complete information necessary to model the percolating network and to work out individual junction behaviour would be available from the combination of the two methods.

The current path reconfiguration itself, however, can be measured quantitatively over the whole network with the BEC-M alone, at various current levels, even at levels as low as nanoampere currents.

The voltage across the circuit ($V(T)$ in Figure 4e) shows a similar behaviour to that observed in Bellew et al.³² The linear I - V regime at low currents and a slight deviation from it at medium current levels is followed by a significant drop after which linearity is regained at larger currents. Such behaviour is considerably different from the case where temperature dependence is not taken into account ($V(T_0)$ in Figure 4e).

From this example, it is clear that the combination of microscopic current density and thermal measurements on percolating networks at various input current levels can help to gain insight into both the individual junction and the overall network behaviour.

BEC-M implementation The creation of the atomic probe for BEC-M requires ultrahigh vacuum environment. To make the instrument compatible with a variety of delicate samples, initial atom trapping and sample probing need to be carried out in distinct regions. We implement the trapping, atomic transport and probing on a single PCB (Figure 5a) allowing for a simple and robust solution.

As pointed out earlier, the spatial resolution (linked to the radial confinement of the atoms) improves as the distance between atoms and the trapping structure decreases. Similarly, the sensitivity to the field or current in the sam-

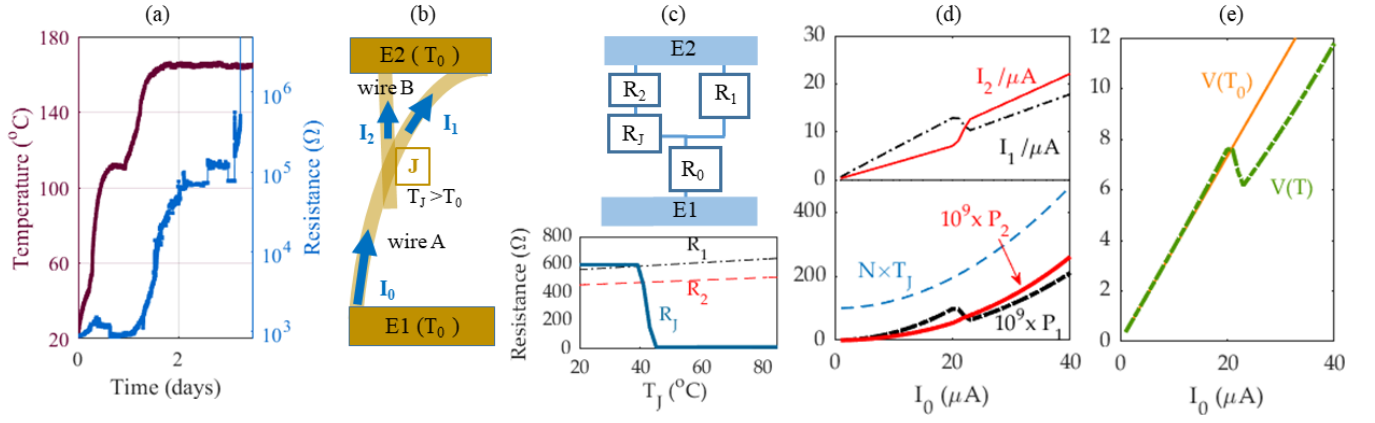


Figure 4: (a) Measurement of a nanowire network resistance while the sample was heated, exhibiting nonlinear response. The abrupt increase in resistance in the final stage is irreversible and corresponds to network failure. (b) Schematic of two wires crossing between two electrodes at a junction. (c) Schematic of the equivalent electrical circuit and the junction resistance (R_J) as a function of the local temperature (T_J) used in the model. For reference, the wire resistances of the upper section of wire A (R_1) and wire B (R_2) are calculated for the same range of junction temperatures. (d) Current (I_1, I_2) and power (P_1, P_2 in Joules per second) in the two upper wire sections of the circuit. The junction temperature as a function of I_0 is shown for reference (scaled by a factor N). (e) Voltage across the circuit, $V(T)$, when taking into account the temperature dependence in the model, and $V(T_0)$, when ignoring it.

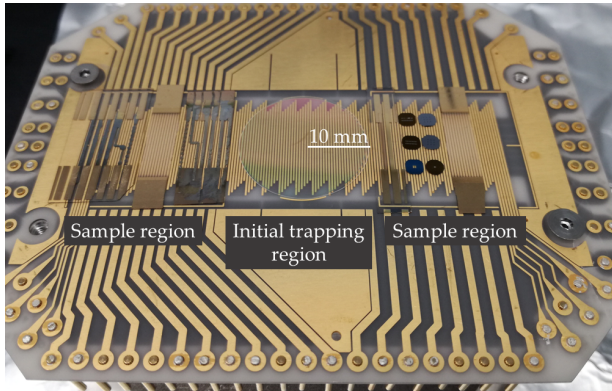


Figure 5: Photograph of a PCB capable of magnetically transporting atoms from the initial trapping and cooling region to the samples, where precise manipulation of the atoms and probing takes place.

ple improves as the atoms approach the surface. In the demonstrations of BEC-M the distance between atoms and surface was near $1\text{ }\mu\text{m}$. Closer approach may be possible, however, trapping atoms at sub-micron distances from a surface poses a challenge due to the strong attractive Casimir-Polder force.³³ For dielectric substrates, a possible solution is the use of evanescent blue detuned light field to compensate for the attractive surface potential.³⁴⁻³⁷ It has also been shown that current in a two-dimensional conductor can trap ultracold atoms with orders of magnitude less spatial noise than with bulk metal trapping wires.³⁸ When implementing such a configuration, it is predicted that the atom-surface distance can be reduced to approximately 100 nm.

It is worth noting, that scattering of ultracold atoms on nano-sized objects can be studied and a scanning probe technique with quantum gases has been introduced for characterizing the electromagnetic properties of nano-structures, including dispersion forces.^{39,40}

As mentioned earlier, the choice of ν_{\perp} , the radial trap frequency, introduces a tunable trade-off between resolution and sensitivity. A pos-

sibility to improve the field sensitivity without compromising the resolution is to change the interaction strength between the atoms. At ultralow temperatures, the interaction between atoms is characterised by the s-wave scattering length a_{sc} , and can be tuned over a large range for example by means of adjusting a bias magnetic field around a Feshbach resonance in optically trapped clouds of atoms.⁴¹ An additional advantage of this implementation is the possibility to take single shot 2D maps of the magnetic field and current density distribution.

Conclusion The BEC-M technique is able to map current patterns at very low current levels - in the nanoampere range - where the sensitivity of thermal imaging methods is not sufficient. At high currents where network failure is likely, the BEC-M takes advantage of the μ s scale imaging duration, which allows for stroboscopic observation of the network dynamics leading to failure.

Our current density characterization will for the first time avoid intermediate assumptions on the link between thermal and conductive properties. Note here the importance of independently assessing current and temperature changes when their relationship is nonlinear. Combined with existing thermal imaging methods^{9–11} this relationship can be studied extensively, including modeling and testing individual junction behaviour and hot spot formation in networks. Insights into the evolution of irreversible mechanisms in the networks will enable a better understanding of material and device failure and therefore aid the development of devices with better macroscopic performance. Beyond current density mapping the BEC-M also allows for studies of atom-surface interactions which may be of great interest for sensing applications with nano-structures.

Acknowledgement The authors gratefully acknowledge financial support through the Strategic Development Fund of the University of Sussex and the UK National Quantum Technology Hub in Sensing and Timing (EPSRC Reference EP/T001046/1). We thank Alan

Dalton and Matthew Large for valuable discussions and Manoj Tripathi for providing AFM data of silver nanowires. We thank Poppy Joshi, Thomas Barrett and William Evans for valuable contributions to the experimental setup.

References

- (1) Chen, R.; Das, S. R.; Jeong, C.; Khan, M. R.; Janes, D. B.; Alam, M. A. Co-Percolating Graphene-Wrapped Silver Nanowire Network for High Performance, Highly Stable, Transparent Conducting Electrodes. *Advanced Functional Materials* **2013**, *23*, 5150–5158.
- (2) Kumar, S.; Murthy, J. Y.; Alam, M. A. Percolating Conduction in Finite Nanotube Networks. *Physical Review Letters* **2005**, *95*, 66802.
- (3) Sysoev, V. V.; Goschnick, J.; Schneider, T.; Strelcov, E.; Kolmakov, A. A Gradient Microarray Electronic Nose Based on Percolating SnO₂ Nanowire Sensing Elements. *Nano Letters* **2007**, *7*, 3182–3188, PMID: 17924710.
- (4) Nair, P. R.; Alam, M. A. Dimensionally Frustrated Diffusion towards Fractal Adsorbers. *Phys. Rev. Lett.* **2007**, *99*, 256101.
- (5) Pimparkar, N.; Kocabas, C.; Kang, S. J.; Rogers, J.; Alam, M. A. Limits of Performance Gain of Aligned CNT Over Randomized Network: Theoretical Predictions and Experimental Validation. *IEEE Electron Device Letters* **2007**, *28*, 593–595.
- (6) Žeželj, M.; Stanković, I. From percolating to dense random stick networks: Conductivity model investigation. *Phys. Rev. B* **2012**, *86*, 134202.
- (7) R. Das, S.; M. S. Mohammed, A.; Maize, K.; Sadeque, S.; Shakouri, A.; B. Janes, D.; A. Alam, M. Evidence of Universal Temperature Scaling in Self-Heated

Percolating Networks. *Nano Letters* **2016**, *16*, 3130–3136.

(8) Kalinin, S.; Gruverman, A. *Scanning probe microscopy: Electrical and electromechanical phenomena at the nanoscale*; Springer, 2007.

(9) Estrada, D.; Pop, E. Imaging dissipation and hot spots in carbon nanotube network transistors. *Applied Physics Letters* **2011**, *98*, 073102.

(10) Maize, K.; Das, S. R.; Sadeque, S.; Mohammed, A. M. S.; Shakouri, A.; Janes, D. B.; Alam, M. A. Super-Joule heating in graphene and silver nanowire network. *Applied Physics Letters* **2015**, *106*, 143104.

(11) Sannicolo, T.; Muñoz-Rojas, D.; Duy Nguyen, N.; Moreau, S.; Celle, C.; Simonato, J.-P.; Bréchet, Y.; Bellet, D. Direct Imaging of the Onset of Electrical Conduction in Silver Nanowire Networks by Infrared Thermography: Evidence of Geometrical Quantized Percolation. *Nano Letters* **2016**, *16*, 7046–7053.

(12) Wildermuth, Microscopic magnetic-field imaging. *Nature* **2005**, *435*, 440.

(13) Yang, F.; Kollár, A. J.; Taylor, S. F.; Turner, R. W.; Lev, B. L. Scanning Quantum Cryogenic Atom Microscope. *Physical Review Applied* **2017**, *7*, 034026.

(14) Taylor, S. F.; Yang, F.; Freudenstein, B. A.; Lev, B. L. A scanning quantum cryogenic atom microscope at 6 K. *SciPost Phys.* **2021**, *10*, 060.

(15) Garnett, E. C.; Cai, W.; Cha, J. J.; Mahmood, F.; Connor, S. T.; Greyson Christoforo, M.; Cui, Y.; McGehee, M. D.; Brongersma, M. L. Self-limited plasmonic welding of silver nanowire junctions. *Nature Materials* **2012**, *11*, 241–249.

(16) Resende, J.; Papanastasiou, D. T.; Moritz, D. C.; Fontanals, N.; Jiménez, C.; Muñoz-Rojas, D.; Bellet, D. Time of Failure of Metallic Nanowire Networks under Coupled Electrical and Thermal Stress: Implications for Transparent Electrodes Lifetime. *ACS Applied Nano Materials* **2022**, *5*, 2102–2112.

(17) Bose, S. N. Plancks Gesetz und Lichtquantenhypothese. *Z. Physik* **1924**, *26*, 178–181.

(18) Anderson, M. H.; Ensher, J. R.; Matthews, M. R.; Wieman, C. E.; Cornell, E. A. Observation of Bose-Einstein Condensation in a Dilute Atomic Vapor. *Science* **1995**, *269*, 198–201.

(19) Dickerson, S. M.; Hogan, J. M.; Sugarbaker, A.; Johnson, D. M. S.; Kasevich, M. A. Multiaxis Inertial Sensing with Long-Time Point Source Atom Interferometry. *Physical Review Letters* **2013**, *111*, 083001.

(20) Canuel, B.; Leduc, F.; Holleville, D.; Gauquet, A.; Fils, J.; Virdis, A.; Clairon, A.; Dimarcq, N.; Bordé, C. J.; Landragin, A.; Bouyer, P. Six-Axis Inertial Sensor Using Cold-Atom Interferometry. *Physical Review Letters* **2006**, *97*, 010402.

(21) Pandey, S.; Mas, H.; Drougakis, G.; Thekkeppatt, P.; Bolpasi, V.; Vasilakis, G.; Poulios, K.; von Klitzing, W. Hypersonic Bose-Einstein condensates in accelerator rings. *Nature* **2019**, *570*, 205–209.

(22) Krüger, P.; Wildermuth, S.; Hofferberth, S.; Andersson, L. M.; Groth, S.; Bar-Joseph, I.; Schmiedmayer, J. Cold atoms close to surfaces: measuring magnetic field roughness and disorder potentials. *Journal of Physics: Conference Series* **2005**, *19*, 56–65.

(23) Schumm, T.; Estève, J.; Figl, C.; Trebbia, J.-B.; Aussibal, C.; Nguyen, H.; Mailly, D.; Bouchoule, I.; Westbrook, C. I.; Aspect, A. Atom chips in the real world: the effects of wire

corrugation. *Eur. Phys. J. D* **2005**, *32*, 171–180.

(24) Wildermuth, S. Sensing electric and magnetic fields with Bose-Einstein condensates. *Applied Physics Letters* **2006**, *88*, 264103.

(25) Krüger, P.; Andersson, L. M.; Wildermuth, S.; Hofferberth, S.; Haller, E.; Aigner, S.; Groth, S.; Bar-Joseph, I.; Schmiedmayer, J. Potential roughness near lithographically fabricated atom chips. *Physical Review A* **2007**, *76*, 063621.

(26) Folman, R.; Kruger, P.; Schmiedmayer, J.; Hecker Denschlag, J.; Henkel, C. Microscopic Atom Optics: From Wires to an Atom Chip. *Advances in Atomic, Molecular, and Optical Physics* **2002**, *48*, 263.

(27) Fortágh, J.; Ott, H.; Kraft, S.; Günther, A.; Zimmermann, C. Surface effects in magnetic microtraps. *Physical Review A* **2002**, *66*, 041604.

(28) Yang, F.; Taylor, S. F.; Edkins, S. D.; Palmstrom, J. C.; Fisher, R., I.; Lev, B. L. Nematic transitions in iron pnictide superconductors imaged with a quantum gas. *Nature Physics* **2020**, *16*, 514–519.

(29) Gerbier, F. Quasi-1D Bose-Einstein condensates in the dimensional crossover regime. *Europhys. Lett.* **2004**, *66*, 771.

(30) Mitchell, M. W.; Palacios Alvarez, S. Colloquium: Quantum limits to the energy resolution of magnetic field sensors. *Rev. Mod. Phys.* **2020**, *92*, 021001.

(31) Large, M. J.; Burn, J.; King, A. A.; Ogilvie, S. P.; Jurewicz, I.; Dalton, A. B. Predicting the optoelectronic properties of nanowire films based on control of length polydispersity. *Scientific Reports* **2016**, *6*, 25365.

(32) T. Bellew, A.; G. Manning, H.; Gomes da Rocha, C.; S. Ferreira, M.; J. Boland, J. Resistance of Single Ag Nanowire Junctions and Their Role in the Conductivity of Nanowire Networks. *ACS Nano* **2015**, *9*, 11422–11429.

(33) Lin, Y.; Teper, I.; Chin, C.; Vuletić, V. Impact of the Casimir-Polder Potential and Johnson Noise on Bose-Einstein Condensate Stability Near Surfaces. *Phys. Rev. Lett.* **2004**, *92*, 050404.

(34) Sagué, G.; Vetsch, E.; Alt, W.; Meschede, D.; Rauschenbeutel, A. Cold-Atom Physics Using Ultrathin Optical Fibers: Light-Induced Dipole Forces and Surface Interactions. *Phys. Rev. Lett.* **2007**, *99*, 163602.

(35) Hammes, M.; Rychtarik, D.; Engeser, B.; Nägerl, H.-C.; Grimm, R. Evanescent-Wave Trapping and Evaporative Cooling of an Atomic Gas at the Crossover to Two Dimensions. *Physical Review Letters* **2003**, *90*, 173001.

(36) Bender, H.; Stehle, C.; Zimmermann, C.; Slama, S.; Fiedler, J.; Scheel, S.; Buhmann, S. Y.; Marachevsky, V. N. Probing Atom-Surface Interactions by Diffraction of Bose-Einstein Condensates. *Physical Review X* **2014**, *4*, 011029.

(37) Landragin, A.; Courtois, J.-Y.; Labeyrie, G.; Vansteenkiste, N.; Westbrook, C. I.; Aspect, A. Measurement of the van der Waals Force in an Atomic Mirror. *Physical Review Letters* **1996**, *77*, 1464–1467.

(38) Sinuco-León, G.; Kaczmarek, B.; Krüger, P.; Fromhold, T. M. Atom chips with two-dimensional electron gases: Theory of near-surface trapping and ultracold-atom microscopy of quantum electronic systems. *Physical Review A* **2011**, *83*, 021401.

(39) Gierling, M.; Schneeweiss, P.; Visanescu, G.; Federsel, P.; Häffner, M.; Kern, D. P.; Judd, T. E.; Günther, A.; Fortágh, J. Cold-atom scanning probe

microscopy. *Nature Nanotechnology* **2011**, *6*, 446–451.

(40) Schneeweiss, P.; Gierling, M.; Visanescu, G.; Kern, D. P.; Judd, T. E.; Günther, A.; Fortágh, J. Dispersion forces between ultracold atoms and a carbon nanotube. *Nature Nanotechnology* **2012**, *7*, 515–519.

(41) Chin, C.; Grimm, R.; Julienne, P.; Tiesinga, E. Feshbach resonances in ultracold gases. *Rev. Mod. Phys.* **2010**, *82*, 1225–1286.